Physica B 690 (2024) 416264

Contents lists available at ScienceDirect

Physica B: Condensed Matter

journal homepage: www.elsevier.com/locate/physb

Some aspects of electron-phonon interaction in $Zn_{1-x}Cd_xGeAs_2$

M. Romcevic [a,*], L. Kilanski [b], M. Curcic [a], N. Paunovic [a], M. Prekajski Đorđević [c], N. Romcevic [a]

[a] Institute of Physics, University of Belgrade, Belgrade, Serbia
[b] Institute of Physics, Polish Academy of Sciences, Warsaw, Poland
[c] Vinca Institute, University of Belgrade, Belgrade, Serbia

ARTICLE INFO

Keywords:
Composite materials
Electron-phonon interaction
Vibrational spectroscopy

ABSTRACT

The interaction between charge carriers and phonons is the primary mechanism through which charge carriers exchange energy with the crystal lattice. A proper understanding of the electron-phonon interaction is of great importance. We conducted a comprehensive investigation to examine the electron-phonon interaction in semiconductor crystals of $Zn_{1-x}Cd_xGeAs_2$ ($0 \leq x \leq 1$). For this objective, X-ray diffraction, far-infrared reflection, and Raman scattering studies were employed. In addition to the two primary phases, namely $ZnGeAs_2$ and $CdGeAs_2$, four component phases were also identified: $ZnAs_2$, $CdAs_2$, GeAs, and $GeAs_2$. A spatially inhomogeneous distribution of charge carriers was detected, with the highest concentration in the vicinity of the formed GeAs. Analysis of the Far-infrared reflection spectrum of $ZnGeAs_2$ ($x = 0$) revealed that plasmon-4 phonon interaction occurs, while in $CdGeAs_2$ ($x = 1$), there is a plasmon-3 phonon interaction. All other samples have both of these interactions, according to their percentage in the composition. Raman measurements revealed that due to the influence of free charge carriers, there is an increase in the intensity of phonon modes, their displacement, or their splitting into two modes. The intensity and the way the electron-phonon interaction vary depending on the local concentration of free carriers, and it is the strongest in the areas around the formed GeAs.

The obtained results and performed analyses revealed the existence of different phases in the material, inhomogeneous charge distribution, and electron-phonon interaction, which are essential properties of thermoelectric materials.

1. Introduction

$Zn_{1-x}Cd_xGeAs_2$ is a semiconductor compound that possesses a crystal structure known as chalcopyrite. It is classified as a member of the II-IV-V_2 ternary semiconductors family, which are widely used in optoelectronic devices like solar cells and light-emitting diodes (LEDs) [1]. The adjustability of the material's composition enables the enhancement of its optoelectronic characteristics. The bandgap of $Zn_{1-x}Cd_xGeAs_2$ can be adjusted extensively (E_g = 0.53–1.15 eV) [2,3] by changing the alloy content, x. With an increase in the value of x, the bandgap of the material lowers, resulting in increased absorption in the infrared region. This semiconductor has unique electronic and optical properties [4,5]. This material demonstrates notable electronic characteristics, including high carrier mobility, low resistivity, and favorable thermal stability [6], rendering it well-suited for high-performance electronic devices. Moreover, a thorough comprehension of its phonon characteristics is crucial for enhancing its efficiency in real-world uses. The phonon properties play a crucial role in determining the heat transfer, mechanical stability, and other important physical qualities.

The interaction between electrons and phonons is a fundamental phenomenon in condensed matter physics, which plays a crucial role in a wide range of physical phenomena [7]. Phonons can interact with electrons in several ways. For instance, as an electron travels through the crystal, it can collide with a phonon, transferring some of its energy to the lattice. On the other hand, when a phonon vibrates, it can produce an oscillating electric field that interacts with the electrons, causing changes in their energy and momentum. This interaction between electrons and lattice vibrations (Electron-phonon interaction) significantly impacts various electronic and optical properties of materials, such as electrical conductivity, thermal conductivity, and superconductivity [8]. Understanding the electron-phonon interaction is crucial for predicting and optimizing the properties of materials in technological applications. In the past decades, significant progress has been made in theoretical and experimental investigations of this interaction [9], leading to a deeper understanding of its underlying mechanisms and effects on the properties of materials. This knowledge has also paved the

* Corresponding author.
E-mail address: romcevic@ipb.ac.rs (M. Romcevic).

https://doi.org/10.1016/j.physb.2024.416264
Received 24 April 2024; Received in revised form 25 June 2024; Accepted 30 June 2024
Available online 2 July 2024

Table 1
List of the $Zn_{1-x}Cd_xGeAs_2$ samples; x is average Cd content; n is Hall carrier concentration.

x	0	0.049	0.155	0.181	0.184	0.656	0.674	1
n [10^{18} cm^{-3}]	5.6	3.8	1.3	6.8	4.5	0.3	0.3	0.3
	p-type			n-type				

way for developing new materials with tailored properties and optimized performance in various applications [10–12]. In this context, a detailed study of the electron-phonon interaction in specific materials, such as $Zn_{1-x}Cd_xGeAs_2$, can provide valuable insights into the fundamental physics of these materials and help optimize their properties for various technological applications.

We examined the $Zn_{1-x}Cd_xGeAs_2$ ($0 \leq x \leq 1$) crystals synthesized using a direct fusion method [13]. Studies on $Zn_{1-x}Cd_xGeAs_2$ semiconductor alloy reveal that it only forms a solid solution within limited composition ranges. Specifically, it exists for x values between 0 to 0.2 and 0.85 to 1 [13]. Therefore, this alloy consists of two phases over almost the entire range of intermediate chemical compositions. These are $ZnGeAs_2$ in which Cd has replaced a part of Zn atoms (up to 20 %) - $Zn(Cd)GeAs_2$, and $CdGeAs_2$ with some amount of Zn (up to 15 %) that have replaced Cd atoms - $Cd(Zn)GeAs_2$. This significantly affects the properties of this material.

Spectroscopic methods of X-ray diffraction, IR reflection, and Raman scattering measurements were used to determine their vibrational properties and relate them to the phase analysis of this complex alloy. Also, with these experimental methods, we gained insight into the interaction of phonons with charge carriers. The analysis of these interactions enables a better understanding of the processes taking place in the material and a better insight into the structural, vibrational, and electronic properties and their mutual interdependence.

This paper presents a detailed study of the phonon properties and electron-phonon interactions of $Zn_{1-x}Cd_xGeAs_2$. Our results provide valuable insights into this material's vibrational and electrical properties.

2. Materials and methods

2.1. Samples preparation

The investigated $Zn_{1-x}Cd_xGeAs_2$ samples were synthesized by the direct fusion method [13]. First, single-phase $ZnAs_2$ and $CdAs_2$ were synthesized by direct interaction of high-purity As with Zn and Cd single crystals [14]. Then the three-component compounds $ZnGeAs_2$ and $CdGeAs_2$ were synthesized by the interaction of Ge with previously obtained $ZnAs_2$ and $CdAs_2$ [15]. Finally, these quality single-phase three-component compounds are mixed in a stoichiometric ratio to obtain four-component $Zn_{1-x}Cd_xGeAs_2$. In the above described manner, our samples were synthesized with varying amounts of Zn to Cd. The value of x is changed from 0 to 1, increasing in steps of 0.1.

Ingots of synthesized crystals were cut into slices about 1.5 mm thick. The energy dispersive x-ray fluorescence (EDXRF) method was used to determine the average chemical composition of the samples. The obtained results are presented in detail in the paper [16].

Representative samples of different compositions of synthesized $Zn_{1-x}Cd_xGeAs_2$ crystals were selected for further analysis by spectroscopic methods. The list is given in Table 1.

2.2. Transport properties

The electrical transport properties of $Zn_{1-x}Cd_xGeAs_2$ alloys are studied in detail in the paper [16] including the Hall effect and resistivity vs magnetic field and temperature measurements. The dependencies of the resistivity ρ_{xx}, the Hall carrier concentration n, and the Hall carrier mobility μ, on Cd content x and temperature T were determined for all samples.

The most important for our research is the change in the concentration of free carriers n as the Cd content in the alloys increases. $ZnGeAs_2$ is a p-type material, as well as the $Zn_{1-x}Cd_xGeAs_2$ samples with a small amount of Cd added ($x < 0.18$). As x increases in that range, the concentration of free carriers decreases from 5.6×10^{18} cm^{-3} for $x = 0$ to 7×10^{17} cm^{-3} for $x = 0.166$. When the amount of Cd increases above $x = 0.18$, the type of charge carriers changes so that all samples become n-type. The concentration of carriers decreases from 6.8×10^{18} cm^{-3} for $x = 0.181$ to about 3×10^{17} cm^{-3} for $x = 1$. The authors [16] assume that the main cause is the existence of positively charged defects, which are both scattering centers and sources of free electrons.

Also, the measurements showed that mobility has a minimum of around $x = 0.3$, while resistance reaches a maximum of around $x = 0.4$. Thermally activated transport of carriers was registered in all investigated samples, with the activation energy of electrical conduction (E_a) in the range of 20–30 meV. These results indicate the thermal activation of carriers from defect states into the conduction band.

Changes in the conductivity type from p to n when increasing the amount of Cd in the material are associated with changes in the crystal structure, various defects, and changes in the structure of the energy bands. This change is sharp and occurs at $x \approx 0.2$ when electroactive defects accumulate. This happens because our samples, which were obtained in the described way, were not processed after growth, so the control of the type and amount of structural defects was reduced. So, the change in conductivity type is related to the change in the type of dominant defects in samples and is a result of the growth thermodynamics.

For further analysis by spectroscopic methods, representative samples of different compositions from $x = 0$ to $x = 1$ were selected. Their list is given in Table 1.

2.3. Experimental methods

Our aim was to study how free charge carriers behave and interact with the crystal lattice in the alloys. To accomplish this, we needed to investigate the crystal structure of these materials and their electrical and phononic properties. We used X-ray diffraction, far-infrared reflectivity, and Raman measurements for that purpose.

The far-infrared reflectivity experiment measures the response from the entire sample, i.e., at the millimeter level, and provides integral results. Raman spectra were recorded from a surface with a diameter of 2 μm, i.e., on the micrometer scale, and we got information about local properties. Also, some phonons are visible only in one of the experiments due to the selection rules. So these two experiments together provide a more complete picture of the optical and electrical properties of the material.

2.3.1. X-ray diffraction

The structural properties of the $Zn_{1-x}Cd_xGeAs_2$ samples were investigated using the XRD powder diffraction technique.

The X-ray diffraction (XRD) data was measured using X-ray diffractometer (XRD) Rigaku Ultima IV, Japan, with Cu Kα radiation at room temperature. For the phase identification and data analysis, the PDXL2 v2.0.3.0 software was used, with reference to the diffraction patterns available in the International Center for Diffraction Data (ICDD) (ICDD (PDF-2 2023)) [17,18].

2.3.2. Infrared reflectivity measurements

Far-infrared (FIR) reflectivity measurements were performed with a BOMEM DA-8 Fourier transform infrared spectrometer. Measurements were performed in the spectral range from 40 to 450 cm^{-1} at room temperature. A Hyper beam splitter and pyroelectric and deuterated triglycine sulfate (DTGS) detector were used.

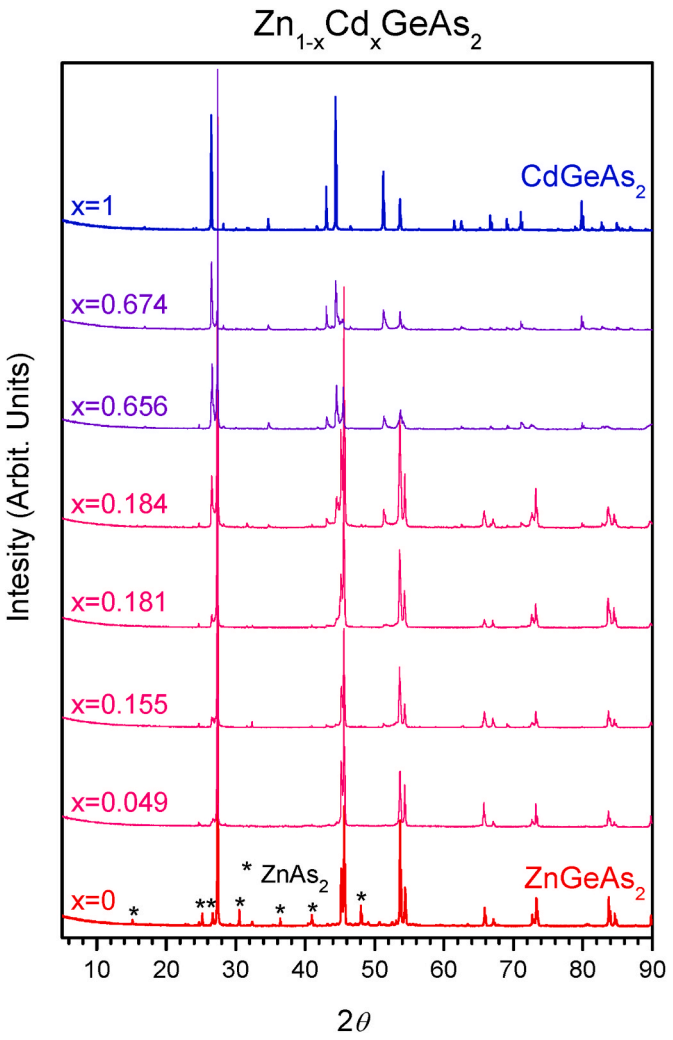

Fig. 1. X-ray diffraction patterns of $Zn_{1-x}Cd_xGeAs_2$ samples ($0 \leq x \leq 1$). Diffraction peaks that correspond to a $ZnAs_2$ phase are marked by asterisks.

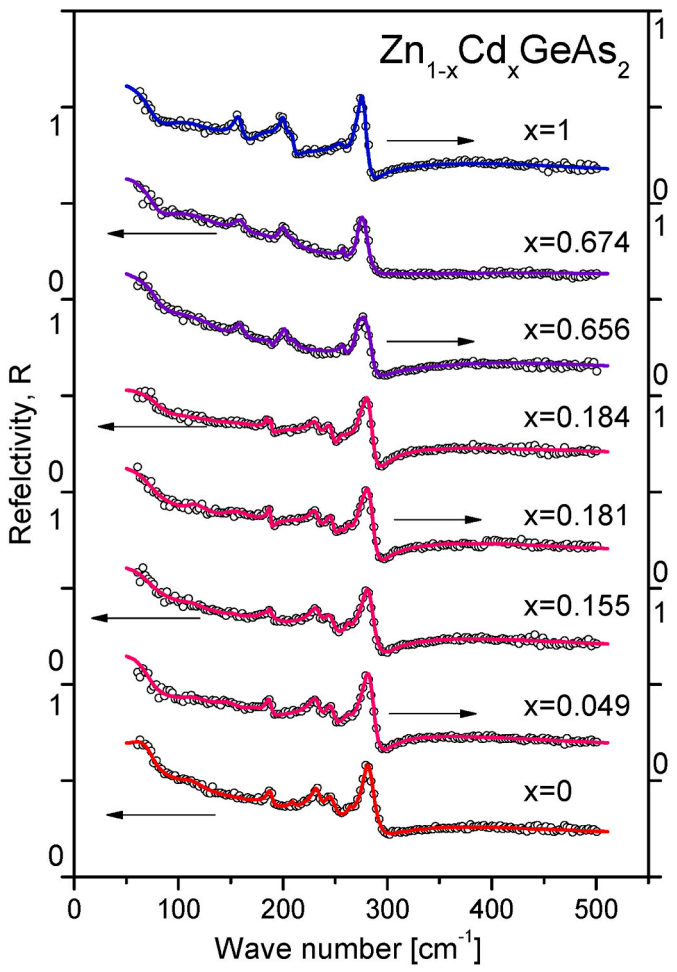

Fig. 2. Far-infrared reflection spectra of the $Zn_{1-x}Cd_xGeAs_2$ samples at room temperature in spectral range 60–500 cm^{-1}. Experimental data are represented by circles, while the solid lines are calculated spectra obtained by a fitting procedure, based on the model for plasmon-phonon coupling (Eq. (2)).

2.3.3. Raman spectroscopy

For further analysis, we used Raman spectroscopy. Measurements were performed using a TriVista 557 Raman system equipped with a nitrogen cooled CCD detector, in backscattering micro-Raman configuration. The 514.5 nm line of an Ar^+/Kr^+ ion gas laser was used as an excitation source. A microscope lens with a 100 times magnification was used to focus the laser beam. Low laser power was used to avoid local heating of the sample. The microscope, which is part of this system, was used to obtain images of the measured surface, size 60 μm by 48 μm.

3. Results and discusion

3.1. X-ray diffraction

X-ray diffraction measurements were made to determine the composition of the samples. The resulting diffraction patterns are shown in Fig. 1.

It was expected that $Zn_{1-x}Cd_xGeAs_2$ exists as single-phase crystal only for x from 0 to 0.2 and for 0.85 to 1 [13], i.e., that Zn or Cd as substitutional elements could enter the lattice up to some specific amount. For other x values, this is two-phase material consisting of $Zn(Cd)GeAs_2$ and $Cd(Zn)GeAs_2$.

Peaks that correspond $ZnAs_2$ phase (Card No. 03-065-2370), marked with asterisks, appeared in the XRD spectrum of $ZnGeAs_2$ (Card No. 01-080-0526). The spectrum recorded for $x = 1$ corresponds to pure $CdGeAs_2$ (Card No. 01-086-5825). The spectra for $0.15 < x < 1$ show two phases' existence.

3.2. Far-infrared reflection spectroscopy

Far-infrared spectroscopy is a very suitable experimental method for determining the vibrational and electrical properties of materials, as well as their interaction. Reflection spectra recorded in the spectral range from 60 to 500 cm^{-1} are shown in Fig. 2.

It was determined that $Zn_{1-x}Cd_xGeAs_2$ mainly consists of two main phases based on $ZnGeAs_2$ and $CdGeAs_2$ and that their share in the material corresponds to the composition (x). Such a structure affects the appearance of the reflection spectra. In the samples with a higher proportion of Zn ($x \leq 0.184$), modes originating from $ZnGeAs_2$ are dominant, at around 65, 232, 244, and 279 cm^{-1} [19], while in those with a higher amount of Cd ($x \geq 0.66$), the modes related to $CdGeAs_2$ stand out, at about 46, 157 and 274 cm^{-1} [19]. Analysis of the spectra revealed that these phonons participate in the plasmon-phonon interaction. Each composition has interactions within both phases, according to the percentage share.

In order to determine the characteristic parameters of the material, it is necessary to perform analysis of the spectra that considers the existence of plasmon-phonon interactions.

Many authors dealt with theoretical models of the dielectric function in bulk materials [20,21]. Reflection spectra can be described by a

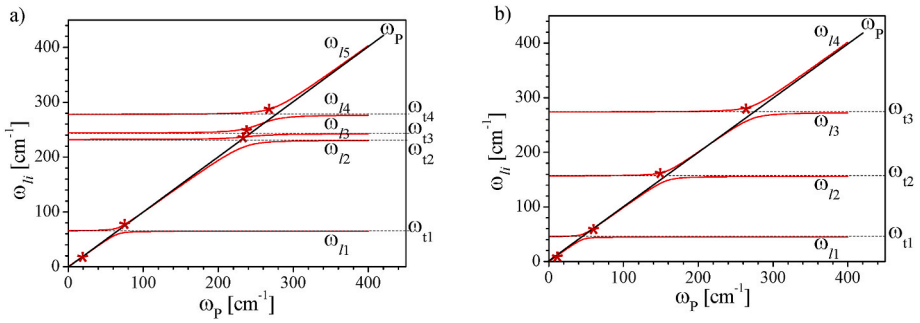

Fig. 3. The eigenfrequencies of the plasmon–multiphonon modes in $Zn_{1-x}Cd_xGeAs_2$ for: a) Zn-rich samples ($x \leq 0.184$) and, b) Cd-rich samples ($x \geq 0.66$). The solid red lines are calculated spectra obtained by the appliance of the model given by Eq. (1) ($Re\{\varepsilon_s\} = 0$), and * represent experimentally values for coupled-mode frequencies determined by Eq. (2). Dotted lines indicate the positions of the initial phonons.

frequency-dependent dielectric function with classical oscillators corresponding to (transverse optical) modes and an associated Drude part that considers the influence of free carriers [22]:

$$\varepsilon_S(\omega) = \varepsilon_\infty + \sum_{k=1}^{l} \frac{\varepsilon_\infty\left(\omega_{LOk}^2 - \omega_{TOk}^2\right)}{\omega_{TOk}^2 - \omega^2 - i\gamma_{TOk}\omega} - \frac{\varepsilon_\infty \omega_P^2}{\omega(\omega + i\gamma_P)} \tag{1}$$

ε_∞ is a bound charge contribution, l is number of phonons, ω_{TOk} and ω_{LOk} are the transverse and longitudinal phonon frequencies, γ_{TOk} is the phonon damping, ω_P is the plasma frequency, and γ_P is the plasma damping. The frequencies of the TO modes are obtained directly using this equation. The values of the LO (longitudinal optical) modes are determined as the maxima of the dielectric loss function.

In the $A_{II}B_{IV}As_2$ group of semiconductor materials, to which $Zn_{1-x}Cd_xGeAs_2$ also belongs, some LO vibration modes are strongly influenced by free carriers, which are described by plasma frequencies ($\omega_p^2 \sim n$) [23,24]. The result is the combined plasmon-LO phonon modes (ω_{lj}), which can be observed in the spectra [23–25]. In that case, it is necessary to remove the influence of free carriers to determine the LO phonon values [26].

Therefore, we decided to use a dielectric function that takes into account the existence of the plasmon-LO phonon interaction to analyze the $Zn_{1-x}Cd_xGeAs_2$ reflectivity spectra:

$$\varepsilon(\omega) = \varepsilon_\infty \frac{\prod_{j=1}^{m+n}\left(\omega^2 + i\gamma_{lj}\omega - \omega_{lj}^2\right)}{\omega^m \prod_{i=1}^{m}(\omega + i\gamma_{Pi}) \prod_{i=1}^{n}\left(\omega^2 + i\gamma_{ti}\omega - \omega_{ti}^2\right)} \prod_{k=1}^{s} \frac{\omega^2 + i\gamma_{LOk} - \omega_{LOk}^2}{\omega^2 + i\gamma_{TOk} - \omega_{TOk}^2} \tag{2}$$

The first fraction in this equation represents the coupled m plasmons and n phonons. ω_{lj} and γ_{lj} are eigenfrequencies and damping coefficients of coupled LO phonons, while ω_{tj} and γ_{tj} correspond to transverse (TO) vibrations. The following factor describes s unpaired modes of the crystal, where ω_{LO} and ω_{TO} are the longitudinal and transverse frequencies, while γ_{LO} and γ_{TO} are damping factors.

The parameters adjustment was carried out using the least-square fitting of theoretical (R) and experimental (Re) reflection coefficients at q points:

$$\chi = \sqrt{\frac{1}{q}\sum_{j=1}^{q}\left(R_{ej} - R_j\right)^2} \tag{3}$$

$$R = \left|\frac{\sqrt{\varepsilon} - 1}{\sqrt{\varepsilon} + 1}\right|^2 \tag{4}$$

where ε is calculated according to Eq. (2). The value of χ was minimized until it reached the standard experimental error (less than 2 %). For all samples, the determination errors of eigenfrequencies were 3–6 %, and for damping coefficients 10–15 %.

Spectra analysis was performed according to the described fitting procedure, and characteristic parameters were detemined. The obtained results are shown in Figs. 3 and 4.

Fig. 3 shows the modes that participate in the plasmon-phonon interaction. The analysis revealed that 4 modes related to $ZnGeAs_2$, namely E^6, E^3, B_2^2, and E^1, and 3 modes of $CdGeAs_2$ – E^6, E^4, and E^1, interact with the plasma. As a result, their LO modes are shifted to slightly higher values. The asterisks show the values obtained as the best fit (Fig. 2) obtained by using the dielectric function Eq. (2).

In principle, the lines representing the coupled mode positions (ω_{li}) are defined as the solutions of a real part of Eq. (1) ($Re\{\varepsilon_S\} = 0$). The solid red lines in Fig. 3a and b were obtained in this way. Dashed lines represent the positions of the initial phonons.

The described results indicate complex interactions between lattice vibrations and free charge carriers. The phonon frequency and the plasma frequency should have close values for their coupling to occur, i. e., each phonon that participates in the interaction with free carriers

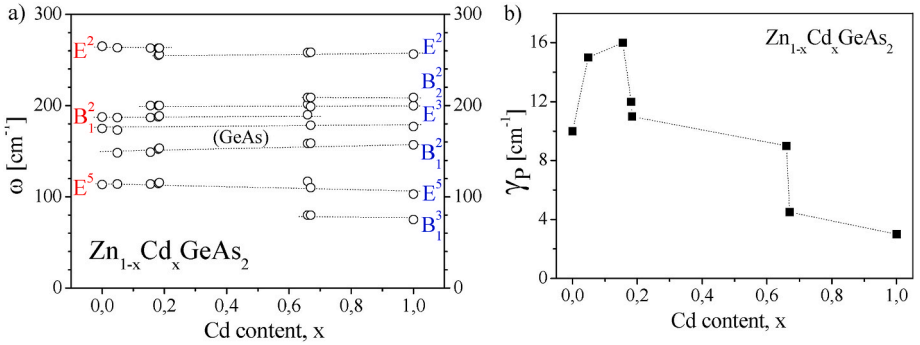

Fig. 4. a) Uncoupled phonons in $Zn_{1-x}Cd_xGeAs_2$, obtained as a result of the best fit (Fig. 2), using the dielectric function Eq. (2); b) the plasma frequency damping (γ_P) depending on the composition of the material. The dotted lines are eye guides.

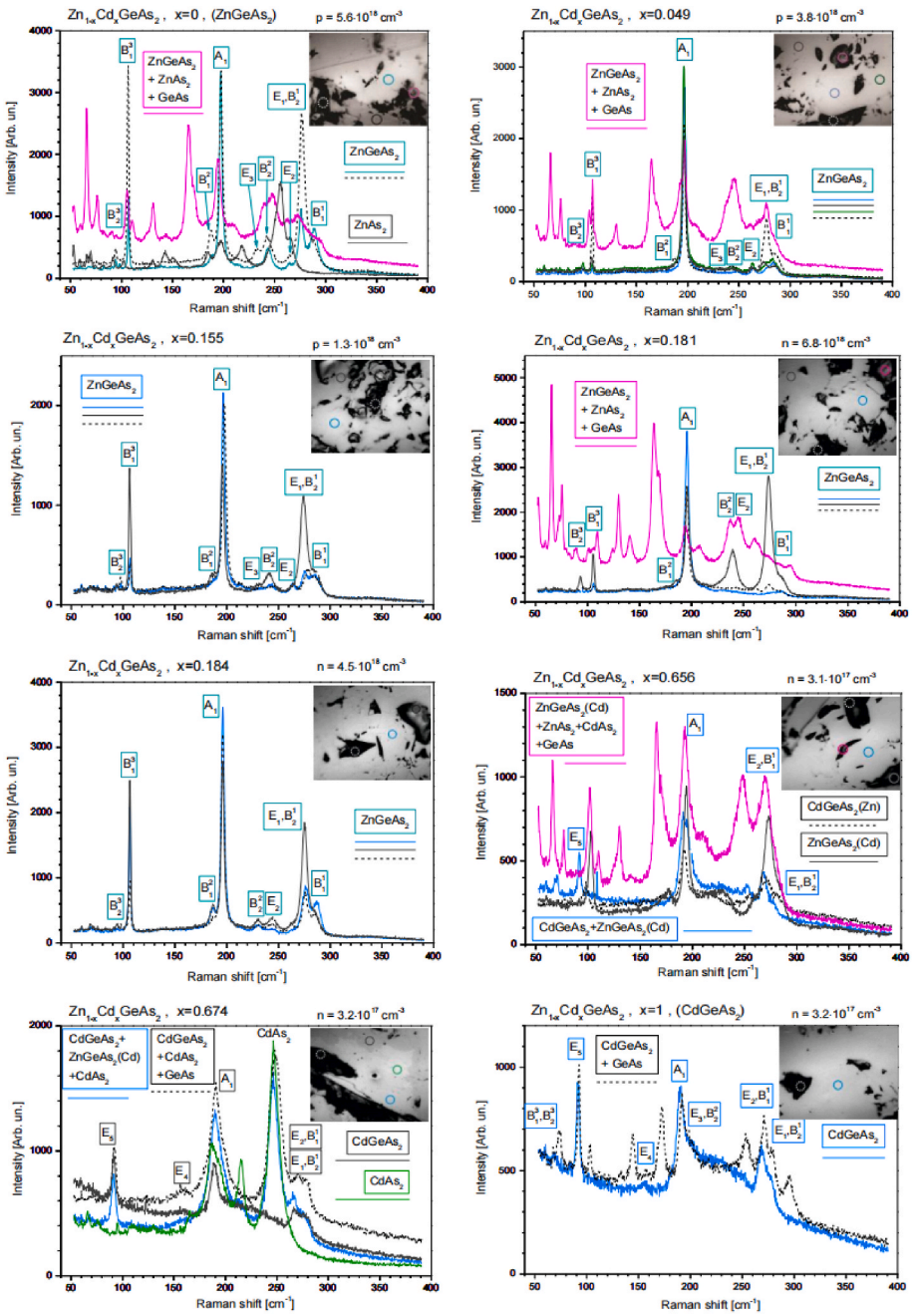

Fig. 5. Raman spectra of $Zn_{1-x}Cd_xGeAs_2$ with different compositions, recorded at room temperature; several spectra were recorded on each sample at characteristic points, marked with small circles of corresponding colors in the images. The size of the images is 60 μm by 48 μm; the $ZnGeAs_2$ and $CdGeAs_2$ modes are marked; the spectra of other existing phases in the material are designated.

"chooses" a plasma frequency close to its own frequency. Since more different phonons interact, means the sample has different plasma frequencies (ω_p) (Fig. 3), i.e., the concentration of free carriers in the sample is inhomogeneous. This is one of the desirable properties of thermoelectric materials.

In addition to the paired ones, there are also unpaired phonons in the material, and their positions are shown in Fig. 4a. They correspond approximately to the values given in the literature for $ZnGeAs_2$ and $CdGeAs_2$ [19], while the intensities of these modes are weak. In the range above 280 cm^{-1}, low-intensity structures originating from multiphonon processes, characteristic of this type of material, can be seen. In addition to the marked phonons originating from $Zn_{1-x}Cd_xGeAs_2$, weak modes at around 152 and 177 cm^{-1} were registered in the entire composition range and could correspond to GeAs [27,28].

One of the parameters determined by the fitting procedure is the plasma damping γ_p. The dependence of γ_p on the composition of the material is shown in Fig. 4b. This parameter increases from x = 0 to 0.155, while it decreases from x = 0.181 to 1. The $Zn_{1-x}Cd_xGeAs_2$ composition for which γ_p reaches a maximum is the same one where the conductivity type changes from p to n [16]. Plasma damping γ_p is related to the lifetime of free carriers (τ^{-1}) and, in principle, is inversely proportional to mobility (μ^{-1}). That indicates that these properties of the material are related to the change in the type of free carriers.

3.3. Raman spectroscopy

Raman spectra were recorded at several characteristic points on each sample, as it is known that the structure of these materials is not

Table 2
Estimated phonon values for $ZnGeAs_2$ [19].

mode	E^6	B_2^3	B_1^3	E^5	E^4	B_1^2	A_1	E^3	B_2^2	E^2	E^1	B_2^1	B_1^1
estimated [cm^{-1}] [19]	76	99	107	114	166	178	199	235	238	268	273	274	275
experimental [cm^{-1}]	–	95	**107**	–	–	187	**197**	233	243	264	**276**, 288		

Table 3
Estimated phonon values for $CdGeAs_2$ [19].

mode	E^6	B_2^3	B_1^3	E^5	E^4	B_1^2	A_1	E^3	B_2^2	E^2	E^1	B_2^1	B_1^1
estimated [cm^{-1}] [19]	46	73	75	96	160	165	196	203	205	268	273	274	275
experimental [cm^{-1}]	–	–	–	**92**	153	–	**191**	200	–	**270**		278	

Table 4
Literature data for phonons of various phases that are present in $Zn_{1-x}Cd_xGeAs_2$ samples.

phase	phonon values [cm^{-1}]
$ZnAs_2$	53, 59, 66, 70, 74, 82, 92, 102, 130, (197), 218, **256**, 266 [29]
$CdAs_2$	186, 190, 194, 214, **246** [30,31]
GeAs	75, 104, 124, 130, 141, **169**, 207, 254, 261 [27,28]
$GeAs_2$	130, **164**, 207 [32]

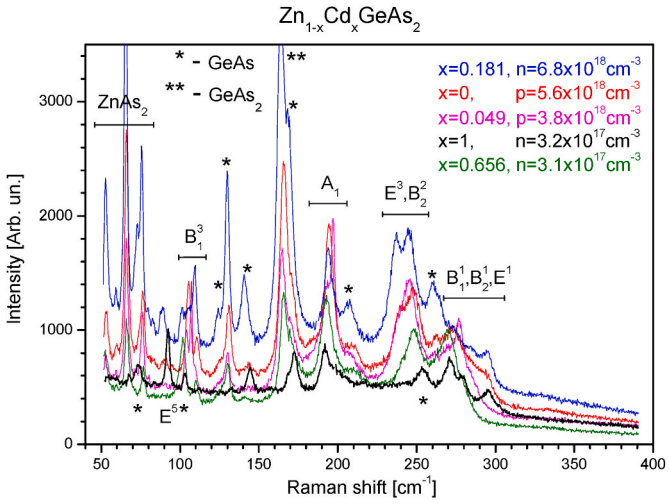

Fig. 6. Spectra recorded at places on the samples where several different material phases are present; The $ZnGeAs_2$ and $CdGeAs_2$ modes are indicated, as well as the peaks corresponding to the $ZnAs_2$ and GeAs phases; The concentrations of free charge carriers in those samples, determined by Hall measurements, are also given.

homogeneous. This was monitored by a microscope that is part of the measuring system. Pictures of size 60 μm by 48 μm were taken, and the spots where Raman spectra were recorded are marked. The diameter of the laser beam is about 2 μm, while the penetration depth is a few μm, and all phases of the material in that volume contributed to the recorded spectrum. Fig. 5 presents the Raman spectra and images of the sample surfaces. The Raman spectra and images of the sample surfaces in Fig. 5 reveal that the light-colored areas on the surface correspond to the basic phases of $Zn(Cd)GeAs_2$ and $Cd(Zn)GeAs_2$, as determined in our previous experiments. The spectra recorded on the dark parts mostly coincide with them, so it is probably the raised parts of the surface. The spectra recorded on the "mixed" parts are rich in modes due to the existence of two-component phases, $ZnAs_2$, $CdAs_2$, and GeAs, whose modes are visible in the spectra.

Tables 2 and 3 provide the values used to mark the modes on the spectra corresponding to the $ZnGeAs_2$ and $CdGeAs_2$ phases. We label spectra recorded at locations where several different phases exist accordingly. The recognition of phases and their labeling was done based on data from the literature, which is given in Table 4.

Fig. 5 shows that the spectra recorded on "mixed" parts of some samples have higher intensities. This is probably related to a higher concentration of charge carriers in those places, which agrees with their already-registered inhomogeneous distribution in the samples. Fig. 6 shows all these spectra together.

Fig. 6 shows that all these selected spectra have a similar shape, i.e., they consist of approximately the same modes. Also, Fig. 6 shows that the intensity of these selected spectra increases with the increase in the concentration of charge carriers (as determined by Hall measurements). The characteristic of these spectra of increased intensity is the existence of GeAs and $GeAs_2$ modes, which are not present in the others. GeAs in the form of a 2D material is an extremely important research topic because it has exceptional properties for applications in optoelectronics and as a thermoelectric material [33–35].

We separated modes using the fitting procedure on all Raman spectra to conduct a more precise analysis. Two analyzed spectra from the group of higher-intensity spectra are shown in Fig. 7. There are narrow phonon

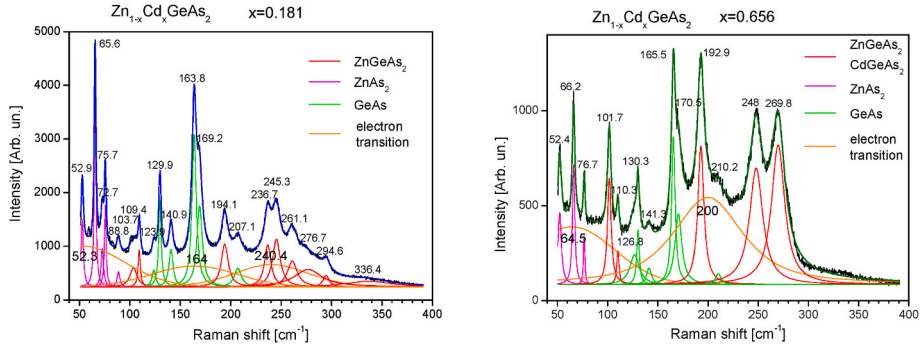

Fig. 7. Characteristic analyzed Raman spectra, recorded in "mixed" fields, with marked phonon modes and electronic transitions.

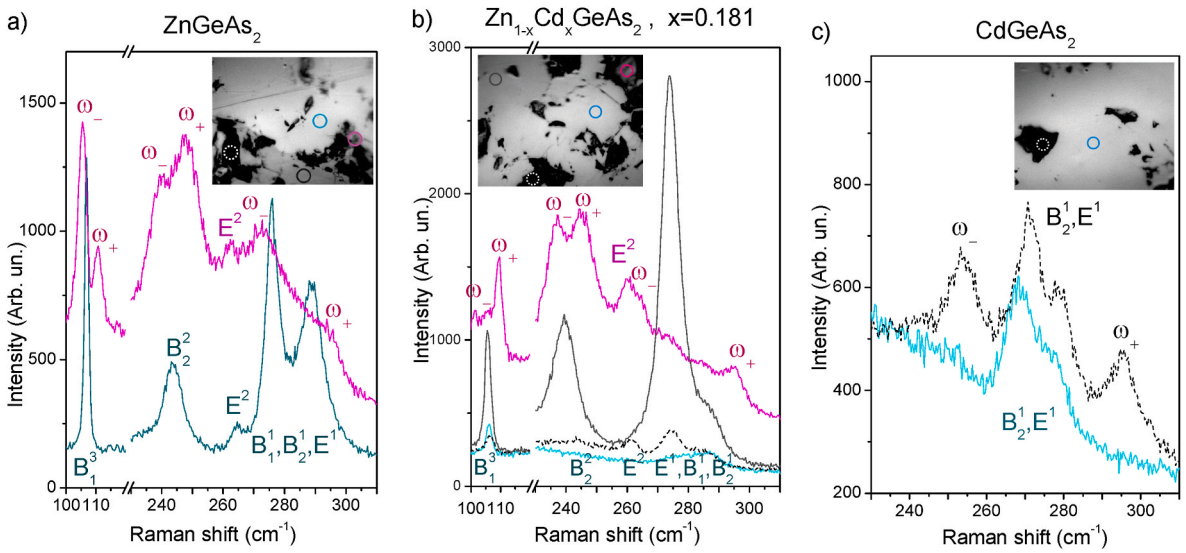

Fig. 8. Examples of electron-phonon interactions; the appearance of ω-and ω_+ modes can be seen in the spectra recorded at places with a higher concentration of free carriers; a) x = 0, b) x = 0.181, c) x = 1; The size of the images is 60 μm by 48 μm.

modes for the two- and three-component phases, as well as broad structures for electronic transitions that need to be taken into account in order to match the experimental and theoretical curves. They also exist on most other spectra but are significantly less intense. Their energies, i.e., the positions on the spectra, approximately coincide with the values of the activation energy of the electrical conduction Ea, which is about 20–30 meV, as determined in the paper [16].

Based on these results, we can associate the higher intensity of electronic transitions with the existence of GeAs and $GeAs_2$ phases. A zone with a higher concentration of free charge carriers forms locally in their environment.

A locally higher concentration of free carriers leads to their interaction with lattice vibrations. One of the results is an increase in the intensity of the modes. Fig. 6 shows an increase in the intensity of the modes for $ZnAs_2$ and GeAs.

Some of the $ZnGeAs_2$ and $CdGeAs_2$ modes behave differently. In their case, electron-phonon interaction occurs. This is seen as amplification, shift, and the appearance of new modes in the Raman spectra, which can be seen in Figs. 6 and 8.

In the spectra recorded at places with high carrier concentration, phonons interacting with charge carriers are divided into two modes – ω-and ω_+. Characteristic examples of the parts of the spectrum where electron-phonon interactions occur are shown in Fig. 8. It can be seen that phonons and charge carriers do not always interact in the same way.

Fig. 8a shows the situation in $ZnGeAs_2$ (x = 0): the B_1^3 mode, located at 107 cm^{-1}, splits into two, at 105.5 and 111 cm^{-1}; B_2^2 goes from 244 to 239.5 and 248.7 cm^{-1}; mode E^2 is weak and moves from 264.3 to 261.7 cm^{-1}, or it also splits into two that are not clearly visible; two peaks at 276 and 288 cm^{-1}, which correspond to the group of close modes B_1^1, B_2^1, and E^1, move to 273 and 295 cm^{-1}, while there is a smooth curve between them and it is not possible to clearly separate individual modes.

In the case of the sample with x = 0.181, the situation is somewhat more complex, as seen in Fig. 8b. Cadmium entered the zinc position in the crystal lattice ($Zn_{1-x}Cd_xGeAs_2$) but not evenly throughout the sample, so regions with a slightly different Cd-composition appear, which can be seen as white and light gray surfaces. Since Cd is a heavier element than Zn, the modes shift to lower values when it enters the lattice. For example, the B_1^3 mode is at 106.4 cm^{-1} for the white field and at 105.7 cm^{-1} for the gray field. Other modes behave similarly. However, when we consider the different local environments and the different concentrations of free carriers per volume of the sample, different electron-phonon interactions are obtained (Fig. 8b). While the intensities of phonons are only increased in the gray fields, in the "mixed" fields, where the concentration of free carriers is significantly higher, the separation of individual modes into two - ω-and ω_+ occurs, in a similar way as for $ZnGeAs_2$ in Fig. 8a. For example, mode B_2^2 is at 244.8 cm^{-1} for the black field, for gray it is at 240.2 with increased intensity, while in the "mixed" field it splits into modes at 236.7 and 245.3 cm^{-1} due to electron-phonon interaction (Fig. 8b).

In $CdGeAs_2$, only modes B_2^1 and E^1 participate in the electron-phonon interaction in the part of the spectrum from 240 to 300 cm^{-1} (Fig. 8c). These modes are located at 268.5 and 273.7 cm^{-1} for white fields, while four values are registered for black fields – 253.7, 271.1, 279.6, and 295.5 cm^{-1}. We assume that the modes B_2^1 and E^1 are divided into - ω-and ω_+. Still, there is also the possibility of seeing modes that do not participate in the interaction but are included in the measurement.

Through this comprehensive analysis of Raman spectra, we determined some properties of the examined $Zn_{1-x}Cd_xGeAs_2$ material that complement those obtained by other experimental methods. The existence of two-component phases $ZnAs_2$, $CdAs_2$, GeAs, and $GeAs_2$ was determined, as well as an uneven distribution of charge carriers, which is extremely high in the GeAs environment, where the strongest electron-phonon interaction occurs.

3.4. Conclusions

The electron-phonon interaction analyzes how the movement of electrons in the crystal and the lattice vibrations interact. This interaction is crucial for understanding the various physical properties of the material.

Analysis of $Zn_{1-x}Cd_xGeAs_2$ crystal lattice revealed the existence of two main phases, $Zn(Cd)GeAs_2$ and $Cd(Zn)GeAs_2$, and several two-component phases - $ZnAs_2$, $CdAs_2$, GeAs, and $GeAs_2$ in almost all samples. A spatially inhomogeneous distribution of charge carriers was registered, with the highest concentration in the vicinity of the formed GeAs.

The electron-phonon interaction was registered in the $Zn_{1-x}Cd_xGeAs_2$ material by both Far-infrared and Raman measurements. Analysis of the Far-infrared reflection spectrum of $ZnGeAs_2$ revealed that plasmon-4 phonon interaction occurs. It involves the phonons E^6, E^3, B_2^2, and E^1, which interact with the plasma, which is inhomogeneously distributed throughout the sample. In $CdGeAs_2$, there is a plasmon-3 phonon interaction in which E^6, E^4, and E^1 phonons participate. All other samples have both of these interactions, according to their percentage in the

composition. Raman measurements showed that due to the influence of free charge carriers, there is an increase in the intensity of the vibrational modes, their displacement, or their splitting into two modes - ω_- and ω_+. Analysis of the Raman spectra revealed that the intensity and nature of interaction vary depending on the local concentration of free carriers.

The established presence of different phases in the material, inhomogeneous charge distribution, and electron-phonon interaction are essential properties of thermoelectric materials. The obtained results and the analyses that were performed will contribute to a better understanding of the structure and processes occurring in II-IV-V_2-type semiconductor materials and the possibilities of their application.

Funding

This research was supported by the Science Fund of the Republic of Serbia, Grant No. 7504386, Nano object in own matrix – Self composite – NOOM-SeC.

CRediT authorship contribution statement

M. Romcevic: Writing – original draft, Methodology, Investigation, Conceptualization. **L. Kilanski:** Writing – original draft, Methodology, Conceptualization. **M. Curcic:** Validation, Methodology. **N. Paunovic:** Validation, Investigation, Formal analysis. **M. Prekajski Đorđević:** Validation, Methodology. **N. Romcevic:** Writing – review & editing, Visualization, Methodology, Investigation, Conceptualization.

Declaration of competing interest

The authors declare that they have no known competing financial interests or personal relationships that could have appeared to influence the work reported in this paper.

Data availability

Data will be made available on request.

References

[1] J.L. Shay, J.H. Wernick, Ternary Chalcopyrite Semiconductors: Growth, Electronic Properties, and Applications, Pergamon, New York, 1975.
[2] V.G. Yarzhemsky, S.V. Murashov, V.I. Nefedov, E.N. Muraviev, Electronic structure and chemical bonds in the magnetic semiconductors Mn_xCd_{1-x} $GeAs_2$ and Mn_x $Zn_{1-x}GeAs_2$, Inorg. Mater. 44 (2008) 1169–1175, https://doi.org/10.1134/S0020168508110034.
[3] H.S. Saini, M. Singh, A.H. Reshak, M.K. Kashyap, Effect of cation substitution on electronic band structure of $ZnGeAs_2$ pnictides: a mBJLDA approach, J. Alloys Compd. 518 (2012) 74–79, https://doi.org/10.1016/j.jallcom.2011.12.129.
[4] R.K. Arslanov, T.R. Arslanov, I.V. Fedorchenko, L. Kilanski, T. Chatterji, Structure-dependent magnetoresistance in the $Zn_{0.1}Cd_{0.9}GeAs_2$+MnAs hybrid nanocomposite, JETP Letters 107 (2018) 612–617, https://doi.org/10.1134/S0021364018100041.
[5] L. Kilanski, P. Skupinski, S. Lewinska, E. Dynowska, A. Reszka, K. Grasza, R. Szymczak, A. Slawska-Waniewska, M. Gorska, B.J. Kowalski, W. Dobrowolski, Homogeneous versus composite $Cd_{1-x-y}Mn_xZn_ySnAs2$ crystals: magnetic interactions and transport properties, Phys. Rev. B 95 (2017) 035206, https://doi.org/10.1103/PhysRevB.95.035206.
[6] S.F. Marenkin, I.V. Fedorchenko, A.D. Izotov, M.G. Vasileva, Physicochemical principles underlying the synthesis of granular semiconductor–ferromagnet magnetic structures exemplified by $A_{II}GeAs_2$ (A_{II} = Zn, Cd) materials, Inorg. Mater. 55 (2019) 865–872, https://doi.org/10.1134/S0020168519090061.
[7] F. Giustino, Electron-phonon interactions from first principles, rev. Mod. Phys. 89, 015003 – published 16 february 2017, Erratum Rev. Mod. Phys. 91 (2019) 019901.
[8] B. Liao, B. Qiu, J. Zhou, S. Huberman, K. Esfarjani, G. Chen, Significant reduction of lattice thermal conductivity by the electron-phonon interaction in silicon with high carrier concentrations: a first-principles study, Phys. Rev. Lett. 114 (2015) 115901, https://doi.org/10.1103/PhysRevLett.114.115901.
[9] M. Cardona, Electron–phonon interaction in tetrahedral semiconductors, Solid State Commun. 133 (2005) 3–18, https://doi.org/10.1016/j.ssc.2004.10.028.
[10] Y. Yamada, Y. Kanemitsu, Electron-phonon interactions in halide perovskites, NPG Asia Mater. 14 (2022) 48, https://doi.org/10.1038/s41427-022-00394-4.
[11] J. Zhou, H.D. Shin, K. Chen, B. Song, R.A. Duncan, Q. Xu, A.A. Maznev, K. A. Nelson, G. Chen, Direct observation of large electron–phonon interaction effect on phonon heat transport, Nat. Commun. 11 (2020) 6040, https://doi.org/10.1038/s41467-020-19938-9.
[12] Y. Quan, S. Yue, B. Liao, Impact of electron-phonon interaction on thermal transport: a review, nanoscale microscale thermophys, Eng. 25 (2021) 73–90, https://doi.org/10.1080/15567265.2021.1902441.
[13] I.V. Fedorchenko, A.N. Aronov, L. Kilanski, V. Domukhovski, A. Reszka, B. J. Kowalski, E. Lahderanta, W. Dobrowolski, A.D. Izotov, S.F. Marenkin, Phase equilibria in the $ZnGeAs_2$–$CdGeAs_2$ system, J. Alloys Compd. 599 (2014) 121–126, https://doi.org/10.1016/j.jallcom.2014.02.085.
[14] S.F. Marenkin, V.B. Lazarev, V.Y. Shievchenko, K.A. Sokolovsky, The growth of $CdAs_2$ and $ZnAs_2$ single crystals by directed zone melting recrystallization, J. Cryst. Growth 50 (1980) 761, https://doi.org/10.1016/0022-0248(80)90024-X.
[15] S.F. Marenkin, V.M. Novotortsev, K.K. Palkina, S.G. Mikhailov, V.T. Kalinnikov, Preparation and structure of $CdGeAs_2$ crystals, Inorg. Mater. 40 (2004) 93–95, https://doi.org/10.1023/B:INMA.0000016079.37020.9d.
[16] L. Kilanski, A. Reszka, M. Gorska, V. Domukhovski, A. Podgórni, B.J. Kowalski, W. Dobrowolski, I.V. Fedorchenko, A.N. Aronov, S.F. Marenkin, Composite $Zn_{1-x}Cd_xGeAs_2$ semiconductors: structural and electrical properties, J. Phys. Condens. Matter 28 (9pp) (2016) 495802, https://doi.org/10.1088/0953-8984/28/49/495802.
[17] Powder Diffraction File, PDF-2 Database, Announcement of New Database Release, International Centre for Diffraction Data, 2012 (ICDD).
[18] C. Suryanarayana, M. Grant Norton, X-Ray Diffraction: A Practical Approach, Springer, New York, 1998. Version 2012.
[19] F.W. Ohrendorf, H. Haeuseler, Lattice dynamics of chalcopyrite type compounds. Part I. Vibrational frequencies, Cryst. Res. Technol. 34 (1999) 339–349, https://doi.org/10.1002/(SICI)1521-4079(199903)34:3<339::AID-CRAT339>3.0.CO;2-E.
[20] E. Burstein, A. Pinczuk, R.F. Wallis, in: D.L. Carter, R.T. Bate (Eds.), The Physics of Semimetals and Narrow-Gap Semiconductors, Pergamon, New York, 1971, p. 251.
[21] M.A. Kinch, D.D. Buss, I.R. Far, Determination of the transverse optic lattice mode in PbTe at low temperature, Solid State Commun. 11 (1972) 319, https://doi.org/10.1016/0038-1098(72)90241-4.
[22] V. Gopal, Analysis of the infrared plasma reflectivity spectra of semiconductors, Infrared Phys. 18 (1978) 121–125, https://doi.org/10.1016/0020-0891(78)90020-9.
[23] N. Romcevic, M. Romcevic, W.D. Dobrowolski, L. Kilanski, M. Petrovic, J. Trajic, B. Hadzic, Z. Lazarevic, M. Gilic, J.L. Ristic-Djurovic, N. Paunovic, A. Reszka, B. J. Kowalski, I.V. Fedorchenko, S.F. Marenkin, Far-infrared spectroscopy of $Zn_{1-x}Mn_xGeAs_2$ single crystals: plasma damping influence on plasmon - phonon interaction, J. Alloys Compd. 649 (2015) 375–379, https://doi.org/10.1016/j.jallcom.2015.07.087.
[24] M. Romcevic, N. Paunovic, U. Ralevic, J. Pesic, J. Mitric, J. Trajic, L. Kilanski, W. Dobrowolski, I.V. Fedorchenko, S.F. Marenkin, N. Romcevic, Plasmon - phonon interaction in $ZnSnSb_2$ + Mn semiconductors, Infrared Phys. Technol. 108 (2020) 103345, https://doi.org/10.1016/j.infrared.2020.103345.
[25] S. Takaoka, T. Hamaguchi, S. Shimomura, K. Murase, Observation of the coupled plasmon-lo phonon mode energy in photo-excited $Pb_{1-x}Sn_xTe$ doped with indium impurities, Solid State Commun. 54 (1985) 99–102, https://doi.org/10.1016/0038-1098(85)91043-9.
[26] A.A. Kukharskii, Plasmon-phonon coupling in GaAs, Solid State Commun. 13 (1973) 1761–1765, https://doi.org/10.1016/0038-1098(73)90724-2.
[27] D.G. Mead, Long wavelength study of semiconducting germanium arsenide, GeAs, Infrared Phys. 22 (1982) 209–213, https://doi.org/10.1016/0020-0891(82)90045-8.
[28] A. Di Bartolomeo, A. Grillo, F. Giubileo, L. Camilli, J. Sun, D. Capista, M. Passacantando, Field emission from two-dimensional GeAs, J. Phys. D Appl. Phys. 54 (2021) 105302, https://doi.org/10.1088/1361-6463/abcc91.
[29] J. Weszka, M. Balkanski, M. Jouanne, D.I. Pishchikov, S.F. Marenkin, Raman scattering in $ZnAs_2$ monoclinic crystals, phys. stat. sol.(b) 171 (1) (1992) 275–281, https://doi.org/10.1002/pssb.2221710130.
[30] J. Weszka, M. Balkanski, A.M. Raukhman, S.F. Marenkin, Raman scattering and lattice vibrations in tetragonal $CdAs_2$ crystals, Phys. Status Solidi 194 (2) (1996) 509–515, https://doi.org/10.1002/pssb.2221940208.
[31] A.I. Ril, I.V. Fedorchenko, S.F. Marenkin, A.V. Kochura, A.E. Kuzko, Phase equilibria in the $CdAs_2$–Cd_3As_2–MnAs ternary system, Russ. J. Inorg. Chem. 62 (2017) 976–986, https://doi.org/10.1134/S0036023617070191.
[32] S. Liu, G. Li, F. Zhu, H. Huang, J. Lu, J. Qu, L. Li, Q. Wen, $GeAs_2$ saturable absorber for ultrafast and ultranarrow photonic applications, Adv. Funct. Mater. 32 (2022) 2112252, https://doi.org/10.1002/adfm.202112252.
[33] J. Guo, Y. Liu, Y. Ma, E. Zhu, S. Lee, Z. Lu, Z. Zhao, C. Xu, S.-J. Lee, H. Wu, K. Kovnir, Y. Huang, X. Duan, Few-layer GeAs field-effect transistors and infrared photodetectors, Adv. Mater. 30 (2018) 1705934, https://doi.org/10.1002/adma.201705934.
[34] L. Liu, V.V. Struzhkin, J. Ying, Pressure-induced superconductivity in GeAs, Phys. Rev. B 100 (2019) 214516, https://doi.org/10.1103/PhysRevB.100.214516.
[35] T. Zhao, Y. Sun, Z. Shuai, D. Wang, $GeAs_2$: a IV–V group two-dimensional semiconductor with ultralow thermal conductivity and high thermoelectric efficiency, Chem. Mater. 29 (2017) 6261–6268, https://doi.org/10.1021/acs.chemmater.7b01343.